Existence and Stability of Localized Oscillations in 1-Dimensional Lattices With Soft-Spring and Hard-Spring Potentials

Panagiotis Panagopoulos
School of Applied Mathematical and Physical Sciences,
National Technical University of Athens

Tassos Bountis
Department of Mathematics and Center for Research and Applications of Nonlinear Systems (CRANS), University of Patras,
GR-26500 Patras, Greece

Charalampos Skokos
Department of Mathematics and Center for Research and Applications of Nonlinear Systems,
(CRANS), University of Patras,
GR-26500 Patras, Greece
and
Research Center for Astronomy and Applied Mathematics,
Academy of Athens, Soranou Efesiou 4
GR-11527, Athens, Greece

In this paper, we use the method of homoclinic orbits to study the existence and stability of discrete breathers, i.e., spatially localized and time-periodic oscillations of a class of one-dimensional (1D) nonlinear lattices. The localization can be at one or several sites and the 1D lattices we investigate here have linear interaction between nearest neighbors and a quartic on-site potential $V(u)=\frac{1}{2}Ku^2\pm\frac{1}{4}u^4$, *where the (+) sign corresponds to "hard spring" and (−) to "soft spring" interactions. These localized oscillations—when they are stable under small perturbations—are very important for physical systems because they seriously affect the energy transport properties of the lattice. Discrete breathers have recently been created and observed in many experiments, as, e.g., in the Josephson junction arrays, optical waveguides, and low-dimensional surfaces. After showing how to construct them, we use Floquet theory to analyze their linear (local) stability, along certain curves in parameter space* (α,ω), *where* α *is the coupling constant and* ω *the frequency of the breather. We then apply the Smaller Alignment Index method (SALI) to investigate more globally their stability properties in phase space. Comparing our results for the* $\pm$ *cases of* $V(u)$, *we find that the regions of existence and stability of breathers of the "hard spring" lattice are considerably larger than those of the "soft spring" system. This is mainly due to the fact that the conditions for resonances between breathers and linear modes are much less restrictive in the former than the latter case. Furthermore, the bifurcation properties are quite different in the two cases: For example, the phenomenon of complex instability, observed only for the "soft spring" system, destabilizes breathers without giving rise to new ones, while the system with "hard springs" exhibits curves in parameter space along which the number of monodromy matrix eigenvalues on the unit circle is constant and hence breather solutions preserve their stability character.* [DOI: 10.1115/1.1804997]

1 Introduction

We consider a one-dimensional (1D) lattice described by the equations of motion:

$$\ddot{u}_n+V'(u_n)=a(u_{n+1}+u_{n-1}-2u_n),\quad -\infty<n<+\infty \qquad (1)$$

where $u_n(t)$ is the displacement of the particle at nth lattice site, a the coupling parameter, and $V(u)$ an on-site potential given by the form

$$V(u)=\tfrac{1}{2}Ku^2\pm\tfrac{1}{2}u^4 \qquad (2)$$

where K>0 is a fixed parameter. Dots indicate time derivatives, and primes differentiation with respect to the argument. These equations describe the dynamics of an infinitely long chain of oscillators, each linearly coupled to its nearest neighbors and experiencing a ''substrate'' potential V. The (+) sign in Eq. (2) implies that the particles are tied to the substrate by ''hard spring'' forces, while the (−) sign refers to the ''soft spring'' case.

Since the seminal paper of MacKay and Aubry in 1994 [1], in which the existence of localized, time periodic solutions (the so-called *discrete breathers*) of systems like (1) was rigorously established, there has been a wealth of results in the physics and mathematics literature, concerning the properties of these solutions (see, e.g., [2–5]). We believe, therefore, that it is timely for the engineering community to become more actively involved in the investigation of these interesting solutions, with the ultimate goal of performing experiments to test the theoretical predictions. It is the purpose of this paper to help make some progress in this direction.

There exist several methods to compute numerically exact breather solutions for system (1) with on site potential (2). With the term ''numerically exact'' breather, we mean a solution that is time-periodic and spatially localized for a lattice of N particles and retains its shape as N is arbitrarily increased. For example, one can use the method of continuation starting from the limit $\alpha=0$, as explained, e.g., in [1] and [4]. On the other hand, it is also possible to apply relaxation methods based on the fact that, if a breather solution exists and is stable, it should attract a region of phase space around it, assuming that some dissipative process is present to eliminate any excess energy [6–8].

In the present paper, we prefer to use the more recently developed method of homoclinic orbits of invertible maps, as described in [9] and implemented in [10–12], which turns out to be very convenient, as it can be applied independently of the value of the coupling parameter α. This method operates in Fourier space and offers excellent approximations for breathers, which can be made ''numerically exact'' by using the convergence of Newton schemes to construct them to arbitrary accuracy. Furthermore, it

Contributed by the Technical Committee on Vibration and Sound for publication in the JOURNAL OF VIBRATION AND ACOUSTICS. Manuscript received August 2003; final revision October 2003. Associate Editor: Alexander F. Vakakis.

provides a systematic way by which all types of breathers possessing an arbitrary number of ''local extrema'' (the so-called multibreathers) can be constructed.

The paper is organized as follows: In Section 2, we describe briefly the method of homoclinic orbits of maps in Fourier space, used to study the existence of breather solutions of our ''hard-spring'' and soft-spring 1D lattices. We explain the notion of resonances between breathers and the ''phonon'' spectrum (the linear mode frequencies of the lattice) and analyze our maps to show that the parameter regions for the existence of breathers in the hard-spring system are much larger than those of the soft-spring case. Our analytical predictions are fully confirmed by numerical experiments, which are presented in Section 3. Incidentally, unlike the discrete case, phonon resonances are very difficult to avoid in continuous systems described by partial differential equations. For an analysis of localized ''waves'' in such systems, see [13].

Subsequently, in Section 4, we examine the local and global stability properties of some of our discrete breathers. Our local analysis is based on Floquet theory and follows the behavior of the eigenvalues of the monodromy matrix of these periodic solutions, as a function of the coupling parameter α and their frequency ω. If all these eigenvalues lie on the unit circle, the breather is said to be locally (linearly) stable, under infinitesimal perturbations, otherwise it is locally unstable.

Thus, by varying the coupling parameter $\alpha>0$, we study the bifurcations (or stability transitions) of breather solutions and discover some important differences in the dynamics of the hard-spring and soft-spring lattice. For example, the hard-spring breathers preserve their stability over much longer parameter intervals and upon bifurcations inherit their stability to new breathers, while the ''soft-spring'' breathers very often undergo complex instability transitions, at which no new periodic solutions arise. We then use the SALI method [14–18] to study solutions more ''globally'' in the vicinity of a breather in the N-dimensional phase space. Thus, we demonstrate the presence of regular motion around stable breathers, while evidence of chaotic behavior is observed at sufficient distance from them in the space of initial conditions.

Finally, in Section 5, we present our conclusions together with some additional results, which show that the energy versus frequency plots for the two systems exhibit quite different characteristics. In the soft-spring lattice, the energy per particle attains a maximum at some frequency value and then decreases towards zero, while for the hard-spring breathers the energy grows monotonically with increasing frequency. It would thus be very interesting to devise actual experiments by which one could test the validity of these results in realistic systems of nonlinear oscillators.

2 The Method of Homoclinic Orbits

Since a discrete breather solution of Eq. (1) is time-periodic with, say, period T and frequency $\omega=2\pi/T$, it can be expanded in Fourier series

$$u_n(t)=\sum_{k=-\infty}^{\infty} A_n(k)\exp(ik\omega t) \tag{3}$$

with coefficients

$$A_n(k)=A_n^*(-k) \tag{4}$$

Since the oscillations are expected to have zero mean, by virtue of the form of the potential (2), we set $A_n(0)=0$. Furthermore, all particles oscillate in phase, hence we may search for solutions with initial velocities zero, thus taking all the $A_n(k)$ to be real numbers. Finally, due to the symmetry of the on site potential (2), only the modes with odd index k (i.e., $k=1,3,5,\ldots$) are nonzero. The existence of such periodic solutions for hard-spring systems [with + in Eq. (2)] has already been extensively demonstrated in the recent literature [9–12].

In this paper, we shall concentrate on the soft-spring potential

$$V(u)=\tfrac{1}{2}Ku^2-\tfrac{1}{2}u^4 \tag{5}$$

Inserting Eq. (3) in the equations of motion (1) and equating coefficients of $\exp(ik\omega t)$ for every k, we obtain the following algebraic system for the $A_n(k)$:

$$A_{n+1}(k)+A_{n-1}(k)=C(k)A_n(k) - \frac{1}{\alpha}\sum_{k_1}\sum_{k_2}\sum_{k_3} A_n(k_1)A_n(k_2)A_n(k_3) \tag{6}$$

where $k_1+k_2+k_3=k$ and

$$C(k)=\left(2+\frac{K-k^2\omega^2}{\alpha}\right) \tag{7}$$

The recurrence relation (6) is an infinite-dimensional mapping of the Fourier coefficients $A_n(k)$ with lattice site index n as iteration parameter. Spatial localization requires that the Fourier amplitudes in the recurrence relation (6) satisfy $A_n(k)\to 0$ as $\|n\|\to\infty$. Hence a discrete (multi-) breather is a homoclinic orbit in the space of Fourier coefficients, i.e., a doubly infinite sequence of points beginning at 0 for $n\to-\infty$ and ending at 0 for $n\to\infty$. Of course, in any numerical method the index space (n,k) has to be restricted to a finite subspace.

Following the above arguments, if the Fourier series of Eq. (4) converges, the $|A_n(k)|$ diminish rapidly with increasing $|k|$, then it is sufficient to consider only a small number of harmonics of Fourier series in Eq. (4), say M, for all n lattice sites ($-\infty<n<+\infty$), i.e., $k=1,2,\ldots,M$. Under these conditions, Eq. (6) represents a $2M$-dimensional map and spatially localized time-periodic solutions may be expected to exist in the neighborhood of the trivial solution ($A_n(k)=0$, for all n, k), provided this solution is hyperbolic, i.e., represents a saddle point of the map.

Thus, we first need to determine conditions under which the trivial fixed point of the $2M$-dimensional map is a saddle and examine the dimensionality of its stable and unstable manifolds. To this end, we observe that a linearization of Eq. (6) near the point [$A_n(k)=0$, for all n, k] yields M uncoupled 2D linear maps with eigenvalues

$$\lambda_{1,2}(k)=\frac{C(k)\pm\sqrt{C(k)^2-4}}{2} \tag{8}$$

for every k. Consequently, the fixed point (0,0) of the map is hyperbolic (saddle point), with an M-dimensional stable and an M-dimensional unstable manifold, if

$$|C(k)|>2, \quad k\in \square \tag{9}$$

The inequality in Eq. (9), using Eq. (7), implies that we must require

$$\omega^2k^2<K \quad \text{or} \quad \omega^2k^2>K+4\alpha \tag{10}$$

Thus, breathers exist if the fundamental frequency ω, obtained from Eq. (7), with $k=1$

$$\omega=\sqrt{K-\alpha(C(1)-2)} \tag{11}$$

and all its harmonics have values outside the range $(K,K+4\alpha)$ specified by Eq. (10). This range, in fact, represents the spectrum of linear modes of the particles (the so-called *phonons*) and is often called the *propagation zone* because it is within this range of frequencies that small disturbances can propagate along the lattice. If ωk were to lie in this range for some k, this would imply the reduction of dimensions of the unstable manifold. Thus, the

origin could not be a saddle fixed point of map (6) and homoclinic points (and breather solutions) would not exist with equivalent properties as $n \to \pm\infty$.

Let us consider now the simplest possible approximation, for which the Fourier series (3) is represented by a single mode only, i.e.,

$$u_n^{(0)}(t) = 2A_n(1)\cos\omega t, \quad -\infty < n < +\infty \tag{12}$$

Substituting Eq. (12) into Eq. (1), using Eq. (2), and scaling also the Fourier coefficients by

$$A_n(1) = \sqrt{\alpha} A_n \tag{13}$$

we obtain, finally,

$$A_{n+1} + A_{n-1} - C(1)A_n = -3A_n^3 \tag{14}$$

where

$$C(1) = \left(2 + \frac{K - \omega^2}{\alpha}\right) \tag{15}$$

Thus, instead of studying the $2M$-D map (6), we solve the 2D map (14) to obtain zeroth order approximations (12) of the breather solutions of the 1D lattice (1) with the quartic on-site potential (2). Clearly, the fixed point (0,0) of the 2D map (14) will be hyperbolic, with a 1D stable and a 1D unstable manifold, if $C(1) > 2$ or $C(1) < -2$. We only treat here the case $C(1) > 2$, because for $C(1) < -2$ the invariant manifolds of the saddle point at (0,0) do not intersect and breathers are not expected to exist.

Using (15), the inequality $C(1) > 2$ means that the value of the frequency ω is below the phonon band (propagation zone), i.e., $\omega^2 < K$. Thus, to have breather solutions, one must appropriately restrict the system's parameters so that the frequencies of all harmonics, $k\omega$, lie outside the phonon band $(K, K + 4\alpha)$. By comparison, the values of the frequencies (fundamental and harmonics) of the hard-spring system are all above the phonon band, once $\omega^2 > K + 4\alpha$ is satisfied. Consequently, the parameter range for the existence of breathers of the hard-spring lattice is much larger than the corresponding one for the soft-spring potential (2).

3 Numerical Computation of Breathers

Let us note now that (14) is an iterative map. This implies that the future state is obtained as the image of the current state and lies in the same 2D space. Starting from an initial point $\mathbf{x}_0 = (A_0, B_0)$ one obtains a unique orbit, denoted by $\{\mathbf{x}_n\}$ with $n \geqslant 0$. The inverse of the map (14) is easily derived

$$\begin{aligned} A_n &= B_{n+1} \\ B_n &= -A_{n+1} + C(1)B_{n+1} - 3B_{n+1}^3 \end{aligned} \tag{16}$$

and, hence, the iteration index n can be any integer ($n \in \mathbf{Z}$) and (14) is called an invertible map. An orbit is also referred as a solution of the map, since it solves the system of Eq. (14). Orbits considered in this paper are orbits connecting the saddle point (0,0) of our map to itself and are called homoclinic orbits. A homoclinic orbit consists by definition of states $\mathbf{x}_n$, which lie at the intersection of unstable manifold and stable manifold of the saddle fixed point. If there is one state for which this holds, there exist infinitely many of them, thus giving rise to an infinity of homoclinic orbits. The emerging picture is that of *a* homoclinic tangle [19].

An example of such a structure is shown in Fig. 1, where we plot in the A_{n+1}, A_n plane the stable and unstable manifolds of the saddle point at (0,0) of 2D map (14) with $C(1) = 3$. Beginning from states close to the origin, which lie on the unstable eigenvector of the Jacobian map of Eq. (14), and applying the map repeatedly, we follow the unstable manifold in the forward direction ($n \to \infty$). We then begin from states close to origin, which lie on the unstable eigenvector of the Jacobian of the inverse map (16), and apply the inverse map to follow the stable manifold in the backward direction ($n \to -\infty$). The plot of our numerical results shows that the manifolds extend to large distances from origin, but also return to form homoclinic points, at the intersections of the stable and unstable manifolds (see Fig. 1). The normalized unstable eigenvector of the Jacobian of map Eq. (14) is given by

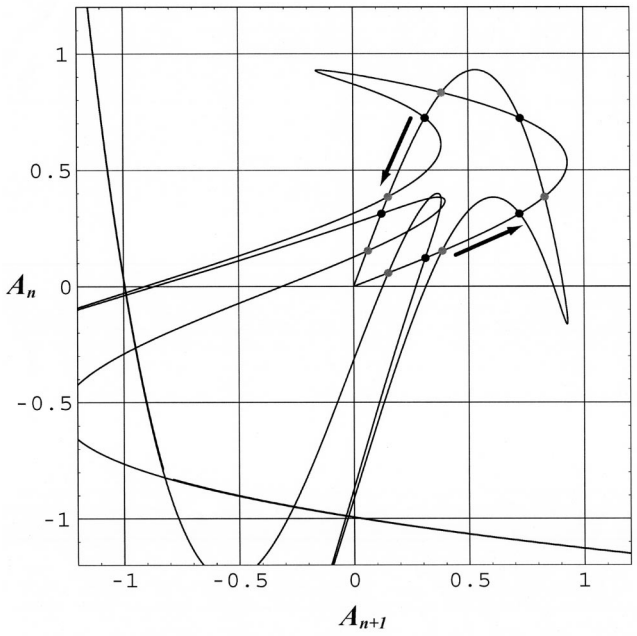

Fig. 1 Part of the homoclinic tangle around the origin of the map of Eq. (16) at $C(1) = 3$. The stable and unstable manifolds are the curves emerging out of the (0,0) saddle point and are indicated by the incoming and outgoing arrows, respectively. Some points of two homoclinic orbits at their intersections (corresponding to two different breather solutions) are shown by dark and gray dots, respectively. They provide very accurate estimates for the oscillation amplitudes A_n of the particles of the lattice, $n \in \mathbf{Z}$.

$$\vec{v} = \begin{pmatrix} v_1 \\ v_2 \end{pmatrix} = \frac{1}{\sqrt{\rho^2 + 1}} \begin{pmatrix} \rho \\ 1 \end{pmatrix}, \quad \rho = \frac{C(1) + \sqrt{C(1)^2 - 4}}{2} \tag{17}$$

and spans the linear unstable eigenspace of the origin. The normalized stable eigenvector of the Jacobian of Eqs. (16) is given by

$$\vec{s} = \begin{pmatrix} s_1 \\ s_2 \end{pmatrix} = \frac{1}{\sqrt{\rho^2 + 1}} \begin{pmatrix} 1 \\ \rho \end{pmatrix} \tag{18}$$

and spans the linear stable eigenspace of the origin. It is well known (see, e.g., [13]) that the stable and unstable manifolds of a hyperbolic fixed point are tangent to the spaces spanned by the stable and unstable eigenvectors of the Jacobian matrix at the fixed point, respectively. It also holds that the Jacobian of the inverse map is the inverse of the Jacobian matrix of the map.

To compute the homoclinic solutions of Eqs. (14) and (16), we apply the following numerical method that uses approximations at the boundaries. We choose $N (-N < n < N)$ for $2N + 1$ particles on the chain and then compute the zeros of an algebraic system. More specifically, due to the topological equivalence of the orbits of the linear system and the complete system we set the $\mathbf{x}_{-N} = (A_{-N+1}, A_{-N})$ state on the linear unstable eigenspace of the origin, i.e., $A_{-N+1} = \varepsilon\gamma v_1$, $A_{-N} = \varepsilon\gamma v_2$, where ε ($|\varepsilon| < 1$) is a scalar parameter, γ is an unknown real number and $v_{1,2}$ are the components of the normalized unstable eigenvector [see Eq. (17)].

Using the same arguments, we set the $\mathbf{x}_N = (A_N, A_{N-1})$ state on the linear stable eigenspace of the origin, i.e., $A_N = \varepsilon\beta s_1$, $A_{N-1} = \varepsilon\beta s_2$, where β is a unknown real number and $s_{1,2}$ are the components of the normalized stable eigenvector, [see Eq. (18)]. Be-

ginning then from state $\mathbf{x}_{-N}$ and applying forward $(F)N-1$ times the recurrence relation (14) we obtain an $A_0^F(\gamma)$ which depends on γ. Repeating the procedure in the backward direction (B), we start from a state $\mathbf{x}_N$. After $N-1$ times we compute the $A_0^B(\beta)$, which depends on β. Since we seek homoclinic orbits, the following relations must be satisfied at the middle of the lattice:

$$A_0^F(\gamma)=A_0^B(\beta) \tag{19}$$

and

$$A_1^B(\beta)=C(1)A_0^F(\gamma)-3(A_0^F(\gamma))^3-A_{-1}^F(\gamma) \tag{20}$$

Thus, the search for homoclinic solutions is reduced to finding a state $\mathbf{x}_{-N}$ of the unstable manifold of the origin and a state $\mathbf{x}_N$ of the stable manifold of the origin, determined by the numbers γ, β, for which Eqs. (19) and (20) are satisfied. There exist several methods for finding zeros of a system of equations like (21), (22) (e.g., Newton methods, steepest descent methods, etc.), but they are not always the most appropriate to employ due to their notorious difficulties in distinguishing between nearby zeros.

Here, we shall use the method of the topological degree [20–22], which gives the exact number of zeros in a restricted interval. It has already been successfully employed for a similar purpose in [10–12], and is ideal for finding zeros when combined with a bisection method (i.e., iteratively dividing the search space in smaller sections containing zeros until each section contains only a single zero and the size of the section is below an accuracy threshold). Finally, to compute the initial positions $u_n(0)$ of the particles for a (multi-)breather solution, we use our homoclinic orbit as a first estimate of the initial positions the $A_n(1)$'s [see Eq. (13)], and insert this set of values as a seed in a Newton-type algorithm (see the Appendix) to find numerically exact breather solutions, like the one shown here in Fig. 2(*a*).

We have also verified, by computing the Fourier amplitudes of the actual breather solutions, that the contribution of higher-order terms grows as the coupling parameter α energy of a breather solution is increased. In particular, in Fig. 2(*b*) we show how the magnitude of $A_0(3)$ increases compared with that of $A_0(1)$. Still, this figure suggests that the higher harmonics, $A_n(k)$, $k>1$, are much smaller than $A_n(1)$ and this justifies our use of the 2D map (14) and explains the accuracy of the approximation (12).

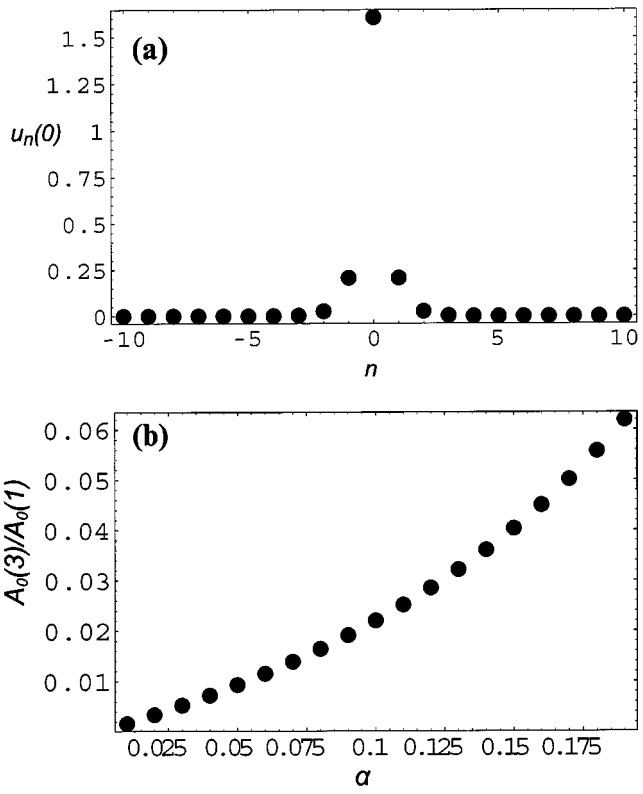

Fig. 2 (*a*) Initial conditions of a simple "soft spring" breather for $K=2$, $C(1)=8$ for 21 particles ($N=10$). (*b*) Variation of the ratio of coefficients $A_0(3)/A_0(1)$ in the Fourier expansion of $u_0(t)$ (position of central particle) versus the coupling parameter α, for the breather in (*a*).

4 Local and Global Stability of Discrete Breathers

For a given solution $\{u_n(t)\}$ of Eqs. (1) and (2) of the soft-spring system, the linearized equations of motion fulfilled by small perturbations $\{e_n(t)\}$ of this solution, are

$$\ddot{e}_n+Ke_n-3u_n^2(t)e_n-a(e_{n+1}+e_{n-1}-2e_n)=0 \tag{21}$$

A solution $\{u_n(t)\}$ is considered stable when, for any initial conditions, the linear perturbations $\{e_n(t)\}$ do not grow exponentially in time. When $\{u_n(t)\}$ is time-periodic with period T, then Eq. (21) defines a linear symplectic map between the initial perturbation at $t=0$ and the perturbation at time $t=T$, expressed by a matrix $F(\{u_n\})$, known as the monodromy matrix:

$$\begin{bmatrix}\{e_n(T)\}\\ \{\dot{e}_n(T)\}\end{bmatrix}=F(\{u_n\})\begin{bmatrix}\{e_n(0)\}\\ \{\dot{e}_n(0)\}\end{bmatrix} \tag{22}$$

The time-periodic solution $\{u_n(t)\}$ is called linearly stable when all the eigenvalues of this monodromy matrix $F(\{u_n\})$ lie on the unit circle. The monodromy matrix $F(\{u_n\})$ always has a pair of degenerate eigenvalues equal to one, corresponding to perturbations in the direction of motion which grow linearly in t. When some eigenvalue pairs "split off" the unit circle, then the corresponding perturbations grow exponentially in time and the breather is called linearly unstable. (For a discussion of all these concepts concerning the linear stability of discrete breathers see [5]).

Using the method of homoclinic orbits described in the above sections, we have constructed a large number of breather solutions of Eq. (1) with the potential (5) and studied their linear stability characteristics. We thus obtained the following results:

- In most cases, as the coupling parameter α increases, breather solutions for soft-spring systems undergo a complex instability transition, i.e., a complex conjugate pair of their eigenvalues achieves magnitudes larger than one by splitting off the unit circle in two complex conjugate pairs [see Fig. 3(c)]. It is important to note that, unlike other bifurcation types (like pitchfork, period-doubling, etc.), this instability transition is not associated with the simultaneous appearance of other (stable) periodic solutions [23,24].
- Unlike the hard-spring case, when we follow curves in the parametric space (α,K,ω), described by the function breather solutions for soft-spring systems do not preserve the number of eigenvalues of the monodromy matrix with absolute values different from one. In Fig. 3 we depict the distribution of eigenvalues of the monodromy matrix for a soft-spring breather solution for various values of coupling parameter a, keeping constant the values for $C(1)$ and for K [see Eq. (15)].

$$G(a,K,\omega)=-\left(2+\frac{K-\omega^2}{a}\right)=\text{const.} \tag{23}$$

By comparison, the breather solutions of systems (1) with quartic hard-spring potential do not appear to exhibit complex instability transitions, as they are always found to become unstable by pairs of eigenvalues splitting off the unit circle at $+1$ on the real axis. Furthermore, they do possess curves in parameter space (α,K,ω), described approximately by Eq. (23), along which

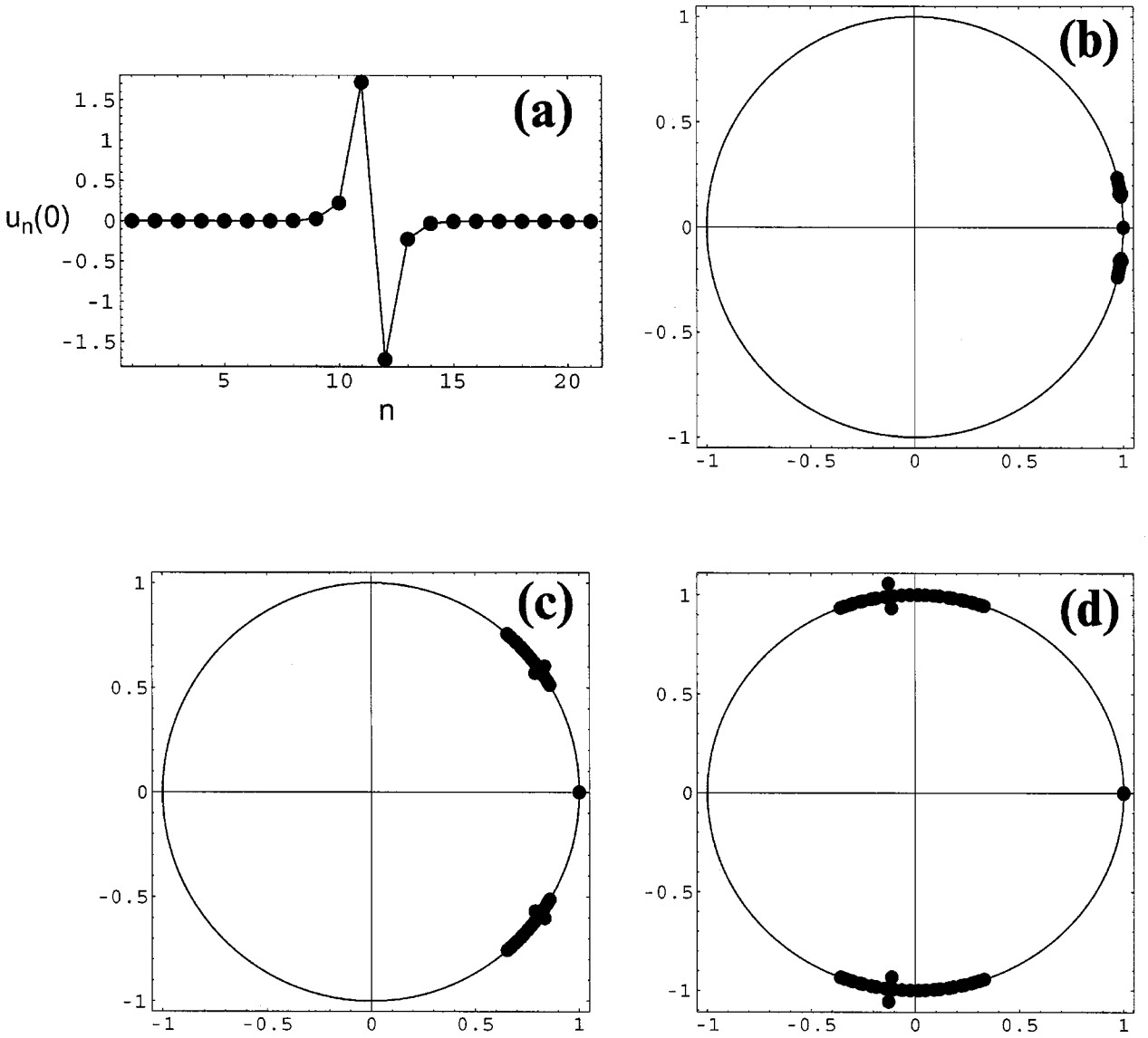

Fig. 3 For the "soft spring" breather shown in (*a*), with 21 particles and $C(1)=8$, $K=2$, we display in the complex plane how the distribution of the eigenvalues of the monodromy matrix changes as the coupling parameter α is increased: (*b*) $\alpha=0.015$, (*c*) $\alpha=0.05$, and (*d*) $\alpha=0.1$. Note the occurrence of complex instability at $\alpha \geqslant 0.05$.

breather solutions do not change their stability preserving the number of eigenvalues of monodromy matrix with absolute values different from one [12,13].

A more "global" investigation of the stability of discrete breathers can be performed using the method of the Smaller Alignment Index (SALI) to discriminate between ordered and chaotic motion in a very efficient way. This method was introduced in [14], where it was applied successfully in 2D, 4D, and 6D symplectic maps. More importantly, however, it distinguishes order from chaos also in Hamiltonian systems, as shown in [15–18], where it was applied to systems with two and three degrees of freedom.

The main advantage of the SALI is that it has completely different behavior for ordered and chaotic orbits, which allows us to decide the nature of the orbit faster than other traditional methods, such as, e.g., the computation of Lyapunov characteristic exponents [25]. In particular, the SALI fluctuates around nonzero values for ordered motion, while it goes abruptly to zero for chaotic orbits. In the latter case, the SALI can also reach the limit of the accuracy of the computer (10^{-16}), which means that the chaotic nature of the orbit is established beyond any doubt and no further computations are needed.

This method can be briefly described as follows: Consider, in an m-dimensional Euclidian space, a nonlinear map T, and the initial condition of an orbit defined by a point $P(0)$. The evolution of this orbit is given by iterating T

$$P(N^*+1)=T(P(N^*)), \quad N^*=0,1,2,\ldots \tag{24}$$

In our case, Eq. (24) represents the numerical integration of Eq. (1), N^* counts the time steps and m is the dimension of the phase space variables $(u_n, \dot{u}_n)$ of the lattice. Solving the linearized equations of motion of Eq. (1) about the orbit $P(N^*)$ yields the linear (tangent) map

$$w(N^*+1)=\left(\frac{\partial T}{\partial P(N^*)}\right)w(N^*) \tag{25}$$

describing the evolution of an initial deviation vector $w(0)$ from the orbit. In order to compute the SALI we follow simultaneously the evolution of $P(N^*)$ and two initially different deviation vectors $w_1(0)$, $w_2(0)$. In every iteration the deviation vectors are normalized, keeping their norm equal to 1, while the norm of their sum (antiparallel alignment index, ALI_+) and their difference (parallel alignment index, ALI_-) are also computed. Then the SALI is defined as the minimum of the following two quantities

$$SALI(N^*) = \min\left\{ \left\| \frac{w_1(N^*)}{\|w_1(N^*)\|} + \frac{w_2(N^*)}{\|w_2(N^*)\|} \right\|, \left\| \frac{w_1(N^*)}{\|w_1(N^*)\|} - \frac{w_2(N^*)}{\|w_2(N^*)\|} \right\| \right\} \tag{26}$$

with $\|\cdot\|$ denoting the euclidean norm.

In the case of chaotic orbits the two deviation vectors will eventually be aligned with the most unstable direction [14], becoming equal ($ALI_- = 0$) or opposite ($ALI_+ = 0$), which means that the SALI becomes zero. The way the two vectors align and, consequently, the way the SALI tends to zero for chaotic orbits was studied in detail in [18]. In particular it was found that the rate at which the SALI tends to zero in the case of chaotic orbits is related to the difference of the two largest Lyapunov characteristic exponents σ_1, σ_2 as SALI$\sim \exp[-(\sigma_1-\sigma_2)t]$ (with t denoting the time).

In the case of ordered orbits on the other hand, the motion is quasiperiodic and takes place on a torus, as if the system were integrable. Thus, any pair of arbitrary deviation vectors tends to the tangent space of the torus and because there is no reason why they should become aligned, in general, they oscillate about two different directions and the SALI fluctuates around some non-zero value. In [17] the behavior of the SALI for ordered orbits was studied and explained, in detail, in the case of a completely integrable 2D Hamiltonian system.

In the present paper we have applied the SALI method to find out how persistent is the ordered behavior around stable breathers in the hard- and soft-spring potentials. Of course, since the numerically exact breathers correspond to periodic orbits in a multidimensional phase space, they can be perturbed by changing a number of different variables. In order to get a rough idea of the "size" of the phase space region of ordered behavior around the stable breather, we have chosen to perturb only the initial position of the central particle u_0.

Thus, starting from the stable periodic orbit and changing u_0 we compute for a sample of orbits the SALI using as initial deviation vectors $w_1(0) = (1,0,\ldots 0)$, $w_2(0) = (0,1,0,\ldots,0)$. The SALI of ordered orbits remains always different from zero exhibiting some small fluctuations. This behavior is shown in the log-log plots of Fig. 4 for the soft-spring potential and Fig. 5 for the hard-spring case, where the SALI of a stable periodic orbit is plotted as function of the number of iterations N^* [curves (a) in both figures].

In the soft-spring case, the first chaotic orbit was found for a perturbation $\Delta u_0 = 0.2207$ and the evolution of the corresponding SALI is plotted in Fig. 4 as curve (*b*). We see that after an initial transient time interval the SALI decreases abruptly reaching very small values, 10^{-10} after $N^* \approx 1500$ iterations, which is the typical behavior of the SALI for chaotic motion.

On the other hand, in the hard-spring case it is much harder to destabilize the stable periodic orbit, as we need a considerably higher perturbation Δu_0 to have chaotic motion. In particular we have to perturb the position of the central particle by $\Delta u_0 = 1.3$ to get a chaotic orbit, the SALI of which is plotted in Fig. 5 as curve (*b*). Again we have an abrupt fall of the SALI to very small values reaching 10^{-10} after $N^* \approx 9500$ iterations.

5 Conclusions

In this paper, we have studied the existence and stability of a physically interesting class of solutions, occurring in nonlinear lattices. These are the so-called discrete breathers, representing localized periodic oscillations, where only a small number of particles at the center of the lattice participate appreciably in the motion, while the amplitudes of all others exponentially decay with respect to their distance from the center. Discrete breathers have recently been created and observed in many experiments, as, e.g., in the Josephson junction arrays [26,27], optical waveguides [28], and low-dimensional surfaces [29]. We have considered 1-dimensional lattices, whose particles are linearly coupled to their nearest neighbors, but also "tied" to a nonlinear substrate potential of the soft-spring type. Since similar studies have been extensively carried out for hard-spring potentials, our aim here was to compare breather dynamics in these cases and identify any physically important differences that may exist.

Our main results can be summarized as follows: Varying the lattice coupling parameter $\alpha > 0$, we have studied bifurcations of several different breather solutions and have found that the hard-spring breathers preserve their stability over much longer parameter intervals and upon bifurcations inherit their stability to new breathers. The soft-spring breathers on the other hand, very often undergo complex instability transitions, at which no new periodic

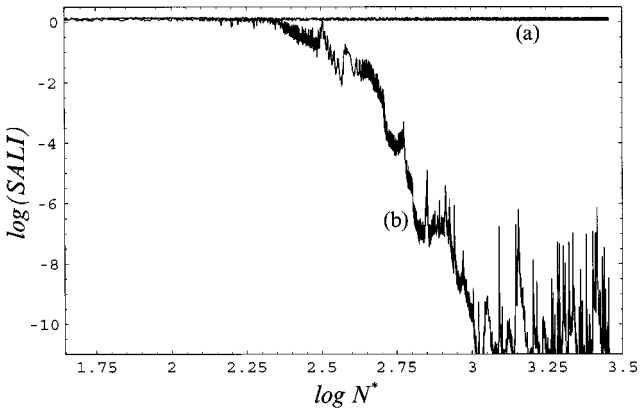

Fig. 4 The log-log evolution of SALI with respect to the number N^* of iterations for the stable breather solution of Fig. 2(*a*) with soft-spring potential containing 21 particles at $C(1) = 8$, $\alpha = 0.15275$, $K = 2$ [curve (a)] and for the same orbit with a perturbation $\Delta u_0 = 0.2207$ in the initial position of the central particle [curve (b)].

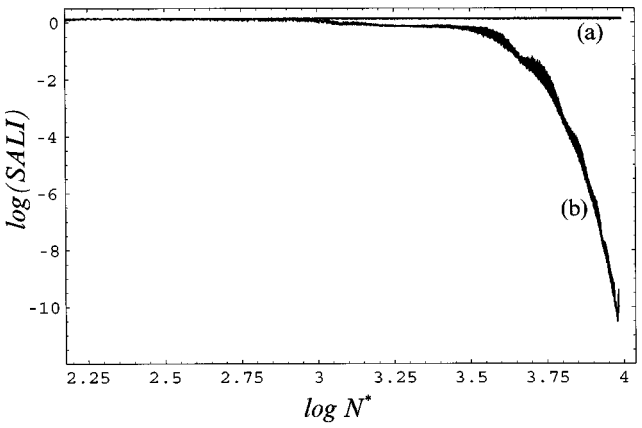

Fig. 5 The log-log evolution of the SALI with respect to the number N^* of iterations for a stable breather, like the one in Fig. 2(*a*), with hard-spring potential containing 21 particles at $C(1) = 8$, $\alpha = 0.15275$, $K = 2$ [curve (a)] and for the orbit with a perturbation $\Delta u_0 = 1.3$ in the initial position of the central particle [curve (b)].

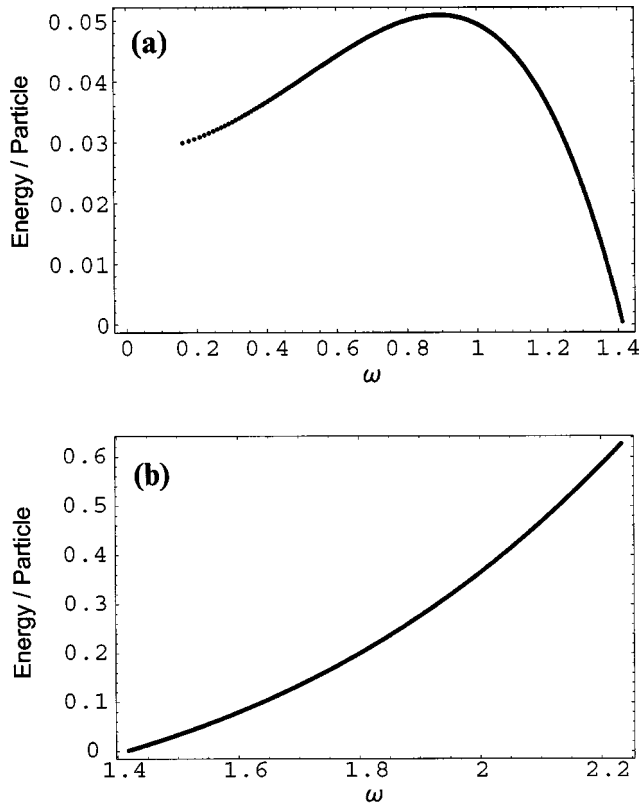

Fig. 6 (*a*) Variation of energy per particle versus frequency ω, for the simple breather with "soft-spring" potential shown in Fig. 2(*a*). (*b*) Variation of energy per particle versus frequency ω, for a simple breather similar to that of Fig. 2(*a*), with "hard-spring" potential, at $K=2$, $C(1)=-8$ and 21 particles.

solutions arise. We have also used the SALI method to examine the presence of ordered or chaotic motion more "globally" in the vicinity of a breather in its multidimensional phase space. Thus, we have observed that regions of regular motion around-stable breathers are considerably larger and evidence of chaotic behavior is observed significantly further from them in the hard-spring lattice, in comparison with similar results for the soft-spring system.

In closing, we would like to point out one more important difference between these two kinds of lattices, regarding the variation of the energy per particle of a breather with the frequency of oscillation ω. In Fig. 6(*a*), we depict this behavior for the soft-spring breather of Fig. 2(*a*) and in Fig. 6(*b*) for a similar breather with a hard-spring potential. In the case of the soft-spring system, the energy per particle exhibits a clear maximum at a frequency below the propagation zone [Fig. 6(*a*)], while the energy of the hard spring is seen to grow monotonically with increasing ω [Fig. 6(*b*)].

This effect is due to the different form of the energy as a function of the coupling constant α in the two cases. Using our simple (but very accurate) approximation (12) with (13), we can express this dependence in the following form [see the potential (2)]:

$$E=\frac{1}{N}\left[a\left(2K\sum_{n=1}^{N}A_n^2\right)+a^2\left(2\sum_{n=1}^{N-1}(A_{n+1}-A_n)^2\pm 4\sum_{n=1}^{N}A_n^4\right)\right] \tag{27}$$

The factor of α^2 in the above function is positive for the hard-spring lattice, while it is negative for the soft-spring system. Now, according to our analysis of Section 2, α is related to ω by the approximate formula (15), which gives for the $C(1)$ and K values of Fig. 6:

- $\alpha=(2-\omega^2)/6$ and $\omega^2<2$ for the soft-spring lattice
- $\alpha=(\omega^2-2)/10$ and $\omega^2>2$ for the hard-spring lattice.

Inserting these expressions for α in (27), it is now easy to explain the main features of the graphs in Fig. 6. For example, in Fig. 6(*a*) the energy starts from a non-zero value and approaches zero as ω tends to $\sqrt{2}$, while in Fig. 6(*b*) ω starts from $\sqrt{2}$ where the energy is zero.

Furthermore, using the above formulas to express the energy E in Eq. (27) as a function of ω^2 it is easy to show that this function has a maximum in the case of the soft-spring lattice, while it grows monotonically for the hard-spring system.

In conclusion, therefore, we believe that our study has revealed some important differences in the dynamics of 1D lattices of nonlinear oscillators with linear coupling among nearest neighbors and soft-spring versus hard-spring on-site potentials. These properties concern the properties of localized periodic oscillations, or discrete breathers, which are currently under study in many physical systems. The fact that these structures are often found to be stable under small perturbations suggests that they may indeed be observable in experimental situations. It would thus be highly desirable to construct such oscillator systems in the laboratory, in one and two spatial dimensions and test the validity of the theoretical analysis and the simulations carried out in this paper.

Acknowledgments

The authors are grateful to the referees for their valuable criticism, which helped us improve significantly the content as well as the presentation of our results. We wish to acknowledge Professor A. Vakakis and J. Bergamin for many useful discussions and comments. Dr. C. Skokos gratefully acknowledges financial support under the "Karatheodory" post-doctoral fellowship No. 2794 of the University of Patras and by the Research Committee of the Academy of Athens.

Appendix: A Newton Algorithm for the Calculation of Breather Solutions of Eq. (1)

In order to compute localized oscillations of period T of the dynamical system described by Eq. (1), with initial conditions $\{u_n(0)\}\neq\{0\}$, $\{\dot{u}_n(0)\}=\{0\}$, we define the following vector equation:

$$\begin{pmatrix}\{u_n(T)\}\\ \{\dot{u}_n(T)\}\end{pmatrix}-\begin{pmatrix}\{u_n(0)\}\\ \{0\}\end{pmatrix}=\vec{P}(\{u_n(0)\}) \tag{A1}$$

where the $\{u_n(t)\}$ represent the positions of the N particles of the system and $\{\dot{u}_n(t)\}$ their velocities at time t. $\vec{P}$ is a $2N\times 1$ vector function of the initial positions $\{u_n(0)\}$.

Since we search for time-periodic solution with zero initial velocities, we need to calculate the N corrections $\{e_n\}$ of the initial positions, in such a way that

$$\vec{P}(\{u_n(0)\}+\{e_n\})=0 \tag{A2}$$

Expanding (A2) around the known quantities $\{u_n(0)\}$, we obtain the following equation:

$$\vec{P}(\{u_n(0)\})+\partial\vec{P}(\{u_n(0)\})(\{e_n\})=0 \tag{A3}$$

where $\partial\vec{P}(\{u_n(0)\})$ is a $2N\times N$ matrix with elements

$$\partial\vec{P}(\{u_n(0)\})_{i,i}=\frac{\partial u_i(T)}{\partial u_i(0)}-1,\quad \partial\vec{P}(\{u_n(0)\})_{i,j}=\frac{\partial u_i(T)}{\partial u_j(0)} \tag{A4}$$

for $1\leq i\leq N$. Observe that the algebraic system (A-3) has $2N$ equations with N unknowns and, hence, is overdetermined. The least squares solution ($\{\overline{e_n}\}$) of Eq. (A-3) satisfies the following equation:

$$\partial\vec{P}^T(\{u_n(0)\})\cdot\partial\vec{P}(\{u_n(0)\})\cdot(\{\overline{e_n}\})$$
$$=-\partial\vec{P}^T(\{u_n(0)\})\cdot\vec{P}(\{u_n(0)\}) \quad (A5)$$

where $\partial\vec{P}^T(\{u_n(0)\})$ is the transpose matrix of $\partial\vec{P}(\{u_n(0)\})$

Thus, the system (A5) contains N equations with N unknowns, which always has a solution when the columns of $\partial\vec{P}(\{u_n(0)\})$ are linearly independent. Solving Eqs. (A5) by a standard numerical scheme, we find the corrections $(\{\overline{e_n}\})$ and calculate new initial positions of the particles by adding these corrections to the old initial positions $(\{u_n(0)\})_{new}=(\{u_n(0)\})+(\{\overline{e_n}\})$. These are now initial guesses for the next step of this Newton algorithm. The procedure is repeated until the calculated initial positions satisfy the relation

$$\vec{P}(\{u_n(0)\}_{new})=0 \quad (A6)$$

within a prescribed accuracy. Thus, the initial positions of the particles for the desired breather solution have been determined.

References

[1] MacKay, R. S., and Aubry, S., 1994, ''Proof of Existence of Breathers in Time-Reversible or Hamiltonian Networks of Weakly Coupled Oscillators,'' Nonlinearity, **7**, p. 1623.

[2] Flach, S., and Willis, C. R., 1998, ''Discrete Breathers,'' Phys. Rep., **295**, p. 181.

[3] Hennig, D., and Tsironis, G., 1999, ''Wave Transmission in Nonlinear Lattices,'' Phys. Rep., **307**, p. 333.

[4] Bambusi, D., 1996, ''Exponential Stability of Breathers in Hamiltonian Networks of Weakly Coupled Oscillators,'' Nonlinearity, **9**, p. 433.

[5] Aubry, S., 1997, ''Breathers in Nonlinear Lattices: Existence, Stability and Quantization,'' Physica D, **108**, p. 201.

[6] Metropolis, N., Rosenbluth, A. W., Rosenbluth, M. N., Teller, A. H., and Teller, E., 1953, J. Chem. Phys., **21**, p. 1087.

[7] Nose, S., 1984, ''A Unified Formulation of the Constant Temperature Molecular Dynamics Method,'' J. Chem. Phys., **81**, p. 511.

[8] Nose, S., 1994, ''A Molecular Dynamics Method for Simulations in the Canonical Ensemble,'' Mol. Phys., **52**, p. 255.

[9] Bountis, T., Capel, H. W., Kollmann, M., Ross, J., Bergamin, J. M., and van der Weele, J. P., 2000, ''Multibreathers and Homoclinic Orbits in 1-Dimensional Nonlinear Lattices,'' Phys. Lett. A, **268**, p. 50.

[10] Bergamin, J. M., Bountis, T., and Vrahatis, M. N., 2002, ''Homoclinic Orbits of Invertible Maps,'' Nonlinearity, **15**, p. 1603.

[11] Bountis, T., Bergamin, J. M., and Basios, V., 2002, ''Stabilization of Discrete Breathers Using Continuous Feedback Control,'' Phys. Lett. A, **295**, p. 115.

[12] Bergamin, J. M., 2003, ''Numerical Approximation of Breathers in Lattices With Nearest-Neighbor Interactions,'' Phys. Rev. E, **67**, 026703.

[13] King, M. E., and Vakakis, A. F., 1994, ''A Method for Studying Waves With Spatially Localized Envelopes in a Class of Nonlinear Partial Differential Equations,'' Wave Motion, **19**, p. 391.

[14] Skokos, Ch., 2001, ''Alignment Indices: A New, Simple Method for Determining the Ordered or Chaotic Nature of Orbits,'' J. Phys. A, **34**, p. 10029.

[15] Skokos, Ch., Antonopoulos, Ch., Bountis, T. C., and Vrahatis, M. N., 2002, ''Smaller Alignment Index (SALI): Detecting Order and Chaos in Conservative Dynamical Systems,'' *Proc. of 4th GRACM Congress on Computational Mechanics*, Vol. IV, D. T. Tsahalis, ed., p. 1496.

[16] Skokos, Ch., Antonopoulos, Ch., Bountis, T. C., and Vrahatis, M. N., 2003, ''Smaller Alignment Index (SALI): Determining the Ordered or Chaotic Nature of Orbits in Conservative Dynamical System,'' Proc. Conference Libration Point Orbits and Applications, G. Gómez, M. W. Lo, and J. J. Masdemont, eds., World Scientific, p. 653.

[17] Skokos, Ch., Antonopoulos, Ch., Bountis, T. C., and Vrahatis, M. N., 2003, ''How Does the Smaller Alignment Index (SALI) Distinguish Order From Chaos?'' Prog. Theor. Phys. Suppl., **150**, p. 439.

[18] Skokos, Ch., Antonopoulos, Ch., Bountis, T. C., and Vrahatis, M. N., 2003, ''Detecting Order and Chaos in Hamiltonian Systems by the SALI Method,'' J. Phys. A, **37**, p. 6269.

[19] Wiggins, S., 1990, *An Introduction to Applied Dynamical Systems and Chaos*, Springer-Verlag, New York.

[20] Vrahatis, M. N., 1995, ''An Efficient Method for Locating and Computing Periodic Orbits of Nonlinear Mappings,'' J. Comput. Phys., **119**, p. 105.

[21] Vrahatis, M. N., 1988, ''Solving Systems of Nonlinear Equations Using the Nonzero Value of the Topological Degree,'' ACM Transcriptions of Mathematical Software, **14**, p. 312.

[22] Vrahatis, M. N., 1988, ''CHABIS: A Mathematical Software Package for Locating and Evaluating Roots of Systems of Nonlinear Equations,'' ACM Transcriptions of Mathematical Software, **14**, p. 330.

[23] Contopoulos, G., 1986, ''Qualitative Changes in 3-Dimensional Dynamical Systems,'' Astron. Astrophys., **161**, p. 244.

[24] Contopoulos, G., 1986, ''Bifurcations in Systems of Three Degrees of Freedom,'' Celest. Mech. Dyn. Astron., **38**, p. 1.

[25] Benettin, G., Galgani, L., Giorgilli, A., and Strelcyn, J.-M., 1980, ''Lyapunov Characteristic Exponents for Smooth Dynamical Systems and for Hamiltonian Systems; A Method for Computing all of Them. Part 2: Numerical Application,'' Meccanica, March, p. 21.

[26] Trias, E., Mazo, J. J., and Orlando, T. P., 2000, ''Discrete Breathers in Nonlinear Lattices: Experimental Detection in a Josephson Array,'' Phys. Rev. Lett., **84**, p. 741.

[27] Binder, P., Abraimov, D., Ustinov, A. V., Flach, S., and Zolotaryuk, Y., 2000, ''Observation of Breathers in Josephson Ladders,'' Phys. Rev. Lett., **84**, p. 745.

[28] Eisenberg, H. S., Silberberg, Y., Morandotti, R., Boyd, A. R., and Aitchison, J. S., 1998, ''Discrete Spatial Optical Solitons in Waveguide Arrays,'' Phys. Rev. Lett., **81**, p. 3383.

[29] Swanson, B. I., Brozik, J. A., Love, S. P., Strouse, G. F., Shreve, A. P., Bishop, A. R., Wang, W.-Z., and Salkola, M. I., 1999, ''Observation of Intrinsically Localized Modes in a Discrete Low-Dimensional Material,'' Phys. Rev. Lett., **82**, p. 3288.